



Morphological and compositional characteristics of bimetallic core@shell nanoparticles revealed by MEIS



Dario F. Sanchez^{a,*}, Raquel Moiraghi^{b,1}, Fernando P. Cometto^{b,2}, Manuel A. Pérez^b, Paulo F.P. Fichtner^{a,c}, Pedro L. Grande^a

^a Instituto de Física, Universidade Federal do Rio Grande do Sul, Porto Alegre, Brazil

^b INFIQC, Departamento de Fisicoquímica, Facultad de Ciencias Químicas, Universidad Nacional de Córdoba, Córdoba, Argentina

^c Department of Metallurgy, Engineering School UFRGS, Porto Alegre, Brazil

ARTICLE INFO

Article history:

Received 17 November 2014

Received in revised form

16 December 2014

Accepted 31 December 2014

Available online 8 January 2015

ABSTRACT

In this paper we report the application of a suitable methodology to study the morphology, structure and composition of core@shell nanoparticles (NPs) systems with polydispersity in the shell thickness, with subnanometer resolution and good sampling. Through the combination of Medium Energy Ion Scattering with Transmission Electron Microscopy, we perform a systematic investigation on core@shell Au@Ag NPs synthesized by an original wet chemical method. For samples synthesized with baths of different AgNO₃ concentrations, the present approach allowed us to determine the NP's Ag shell thicknesses distribution of about a few nanometers around the Au core.

© 2015 Elsevier B.V. All rights reserved.

Keywords:

MEIS

Polydisperse nanoparticles

Core@shell nanoparticles

Au@Ag nanoparticles

1. Introduction

The particular optical properties of colloidal metallic nanoparticles (NPs) have been applied on glass technologies for thousands of years in the human history. Particularly, the use of NPs composed by gold and silver in glasses has been noticed since the Roman era [1]. Nowadays, bimetallic NPs still are of immense interest from both, the scientific and the technological points of view, since their physical properties can be controlled by tuning the NP characteristics such as size, shape, composition, crystallinity and surface properties. Bimetallic core@shell NPs form an important class of nanostructures whose applications are linked to catalysis, cancer immunotherapy, hydrogen fuel-cell devices and plasmonics among others [2–10]. In these systems, each NP has a multicomponent nature and its parameters can be individually tuned to manipulate

the desired properties accordingly with a specific application. For example, the control of Ag shell thickness in Au@Ag NPs systems allows the tuning and enhancement of the Ag resistance to oxidation, which is important for the development of plasmonic sensors [8]. Irrespective to the wide variety of synthetic procedures available in literature [11,12], the formation mechanisms of core@shell NPs and even single-component NPs have been much less investigated. Therefore, the understanding of how several synthesis parameters operate is limited and so is the control over the characteristics of the NPs. The mechanistic studies require an accurate characterization of the properties of the produced NPs as a function of the synthesis conditions in order to unravel the physicochemical processes involved in their formation. A reliable characterization is necessary to precisely determine the relations between the structure of the NPs and their particular properties. Therefore, the developments of suitable techniques which allow the investigation of the NPs morphology, structure and composition with subnanometric resolution and good sampling, is a mandatory requirement [13]. Within this context, UV-Vis spectroscopy has been successfully employed to qualitatively characterize Au@Ag NPs owing to their plasmonic properties [14–16]. However, the quantitative morphological and compositional characterization by this technique has not been informed. Mainly, the difficulties for obtaining data about the morphology and the composition of NPs from UV-Vis are due to the need for a theoretical modeling of

* Corresponding author. Current address: DRT/LETI/DTSI/SCMC, Commissariat à l'énergie atomique – CEA, 17 Rue des Martyrs, Grenoble 38000, France.

Tel.: +33 438789864.

E-mail addresses: dario.f.sanchez@gmail.com, Dario.FERREIRASANCHEZ@cea.fr (D.F. Sanchez).

¹ Current address: Instituto de Física de Rosario, Universidad Nacional de Rosario, Rosario, Argentina.

² Current address: École Polytechnique Fédérale de Lausanne, Laboratory of Nanoscale Science, Lausanne, Switzerland.

the spectra. Furthermore, Transmission Electron Microscopy (TEM) is the most commonly used technique for the study of the morphology and composition of Au@Ag NPs since the NPs can be individually analyzed and no modeling is needed. Conventional TEM, High Resolution TEM (HRTEM) and Scanning TEM with High-Angle Annular Dark-Field (STEM-HAADF) imaging in combination with Energy Dispersive X-ray Spectroscopy (EDS) technique have been successfully applied to resolve individual Au@Ag NPs shape, sizes of the Au core and the Ag shell as precisely identify well as their local composition [2,7–9,17–19]. However, a poor sampling is normally achieved since the analysis is usually performed only over tens to a few thousands of NPs. This restricts the TEM statistical analysis to samples that are nearly-monodisperse since, if the sample is polydisperse, the analysis would be unreliable. As a consequence, synthesis protocols which drive to polydisperse samples are limited to a merely qualitative analysis by the conventional techniques. With the lack of information, conclusions about the factors which contributes to a decreasing of sample quality may be lost and, also, the underlying mechanisms. The Medium Energy Ion Scattering (MEIS) technique, on the other hand, typically probes a sample area of about 10^8 times higher than TEM [20–22]. In addition, its use to analyze nanostructured systems has drawn great attention due to its potential as a tool for the characterization of the shape, size, local composition and stoichiometry of NPs systems [23–26]. Particularly on core@shell NPs, it has been recently demonstrated that MEIS is a powerful technique to investigate their compositional and morphological properties, such as the size of the core, thickness of the shell, as well as their local compositions with sub-nanometer resolution [27,22,26,28]. In addition, the recent development of the PowerMEIS software has expanded the possibilities of using MEIS, allowing to simulate and model MEIS spectra of any kind of nanostructured system, of any kind of shape, composition and spatial distribution [20,21,22,29,30].

In the present work we have extended the application of MEIS to a systematic investigation of the morphological and compositional properties of Au@Ag NPs which are polydisperse in both, morphology and composition. The Au@Ag NPs were produced by chemical reduction of water soluble metal salts precursors in a seed-mediated approach. Through the TEM observations, the typical average NPs sizes and shapes were obtained, which allowed the definition of a geometrical model to be used as an input for the MEIS analysis with PowerMEIS. The local compositional and morphological parameters were later refined. Following this procedure, the size distribution of the seed Au NPs was obtained; the formation of single Ag NPs in addition to a Ag layer on the Au NPs were identified, and the Ag shell thickness and its dispersion were determined.

2. Experimental

Au NPs seeds synthesis (s112): 1 mL of 0.1 M NaBH₄ ice cold solution was added under vigorous stirring into 50 mL of 0.2 mM HAuCl₄ and 2 mM HAc (Acetic Acid) aqueous solution heated up to 90 °C. The heating was kept for 30 min until reaction was complete. The Au NPs obtained are named hereafter as “seeds” or “gold seeds”.

Au@Ag NPs synthesis: core@shell NPs were synthesized by using a seed mediated approach, where gold seeds are added into reactive solutions (baths) for the silver deposition to take place. A typical bath is a solution containing AgNO₃ and a mild reducing agent in acid pH values. In this work the baths were formed by a 0.5 mM NH₃/2 mM HAc buffer (pH ~ 6), 0.1 mM Hydroquinone (H₂Q) and variable AgNO₃ concentration: 0.02 mM (s113), 0.03 mM (s114) and 0.04 mM (s115). In these solutions nucleation of Ag NPs does not occur for at least a few hours as the spectroscopic evidence suggests.

In all cases, core@shell NPs were obtained by adding 0.1 mL of the gold seed suspension into 10 mL of the bath under stirring. The reaction was complete after approximately 2 h, after which stage no significant changes were detected in the spectroscopic signal.

Routine characterization: The extinction spectra of the NPs were recorded using a Shimadzu UV-1200 spectrometer with a 1 cm quartz cell at room temperature. For the morphological characterization, several Transmission Electron Microscopy (TEM) measurements were taken in a JEM-JEOL 1120 microscope employing an 80 kV accelerating voltage. TEM samples were prepared without any purification treatment by seeding many drops of the colloidal solutions onto a Formvar-carbon-covered copper grid and evaporating the water in air at room temperature.

MEIS characterization: The MEIS measurements were performed using a 151.9 keV He⁺ beam from the 500 kV electrostatic accelerator at the Ion Implantation Laboratory, Institute of Physics – UFRGS. The samples were mounted in a 3-axis goniometer inside the analysis chamber kept under a pressure of about 10^{-7} mbar. Typical beam current was less than 15 nA. The normal incidence was used and backscattered He⁺ ions emerging from the target were analyzed using a Toroidal Electrostatic Analyzer (TEA) mounted at 120° with respect to the beam direction. At the top end of the TEA a set of two microchannel plates coupled to a position-sensitive detector allows each ion to be energy- and angle-analyzed leading to 2-D spectra. The TEA angular aperture is 24° and each angle bin corresponds to 0.08°. The overall energy resolution of the system is 500 eV. Details of the data analysis are described in Refs. [20,21,22,29,28]. The ion scattering intensities were analyzed by using the PowerMEIS program [29]. This software calculates the ion scattering intensities as a function of the backscattering energy and angle. For this purpose, the sample is discretized in space by using 3D matrices, where each matrix element stands for specific composition, stoichiometry and density of the material. In this way the set of NPs was generated with specific shapes, size and pair correlation function. The PowerMEIS program can handle any geometric shape, size distribution, and density of the nanostructures. It also accounts for the asymmetry of the energy loss-distribution due to the backscattering collision and also multiple scattering effects.

MEIS samples preparation: Si/SiO₂ wafers were functionalized with APTES (3-Aminopropyltriethoxysilane) in order to improve the binding of NPs to the surface. The Si/SiO₂ functionalized wafers were prepared by immersion in ethanol and ultrasonication during 2 h, then the wafers were immersed in a toluene 1% APTES solution by 30 min. After, the wafers were rinsed with ethanol and milli-Q water. To bind NPs to the substrate surface, the functionalized wafers were immersed by 24 h in the NPs solutions; finally they were washed with milli-Q water and dried at room temperature before the MEIS measurements. The samples' morphology was characterized by atomic force microscopy (AFM) using a Bruker-Innova system in tapping mode at air. The topological images were processed with the WSxM 5.0 software [31]. The AFM images indicate that NPs are attached in an homogenous distribution onto the surface with very little aggregation (see Fig. S1 on the Supporting Information).

3. Results and discussion

Fig. 1a shows a typical TEM image of the sample containing Au NPs seeds whereas in **Fig. 1b** is shown its size distribution. The NPs appear to be small spheres with a narrow size distribution, with radius of (3.5 ± 0.6) nm.

Fig. 2a shows the extinction spectra corresponding to Au@Ag NPs obtained by varying the baths' AgNO₃ content (lines blue, green and black). If compared this spectra with those of the seeds NPs (red line), the Surface Plasmon Resonance (SPR) peak associated to

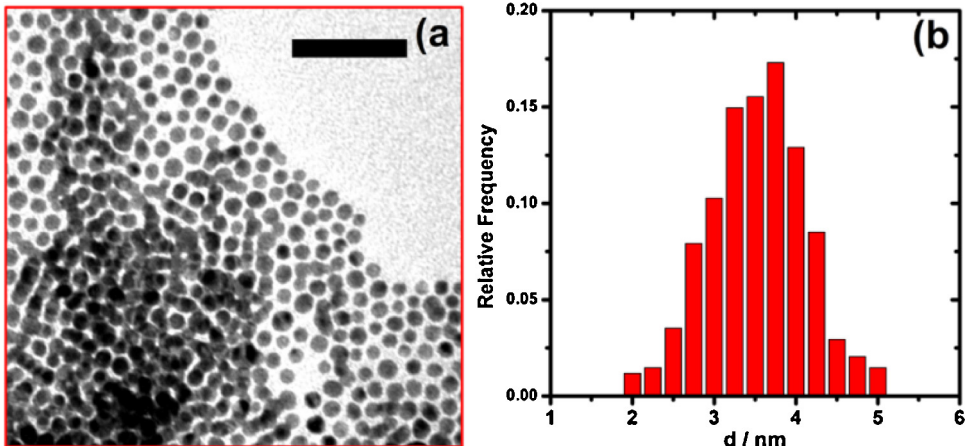


Fig. 1. (a) TEM image of the Au NPs seeds (sample s112). Scale-bar: 50 nm. (b) Size distribution obtained from TEM results.

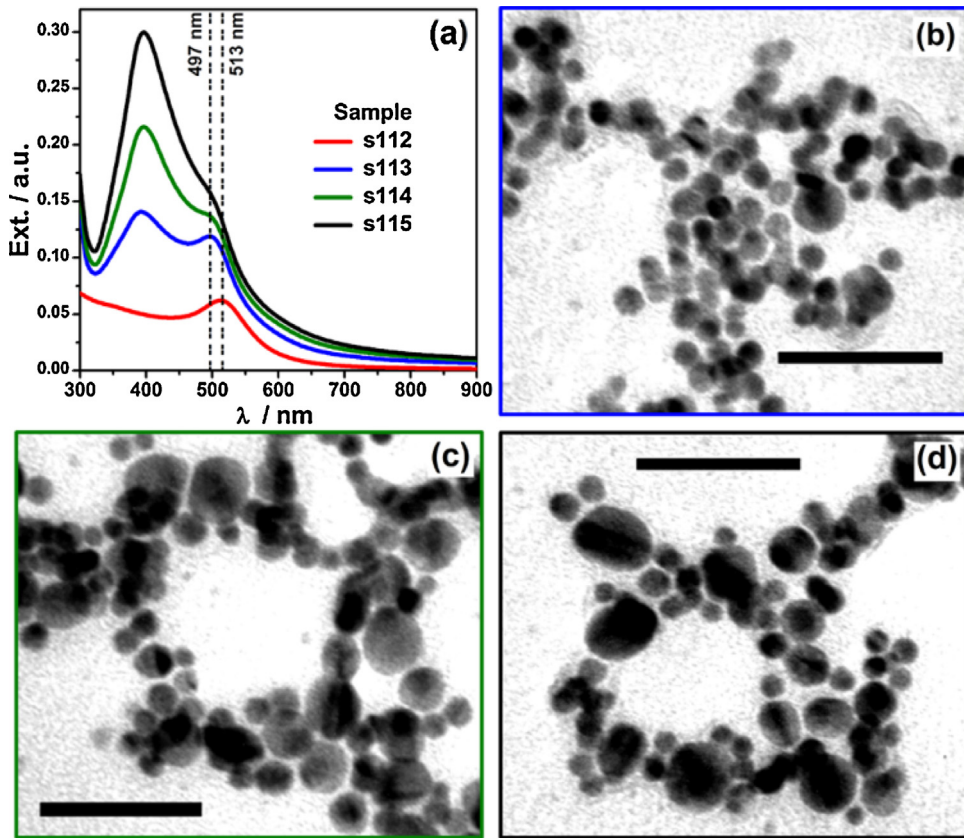


Fig. 2. (a) UV–Vis spectra of the Au@Ag NPs prepared with baths of variable AgNO_3 content (0.02 mM for s113, 0.03 mM for s114 and 0.04 mM for s115) and the spectrum of the Au NPs seeds with the same dilution as in the baths (s112). TEM images of s113 (b), s114 (c) and s115 (d) Au@Ag NPs samples (the same color is used for each specimen's spectrum and image frame). Scale bars: 50 nm.

gold (at ca. 520 nm [32]) is blue shifted for over 16 nm in all cases. This feature indicates that silver is deposit onto the Au NPs surface [14–16] since such a great shifting cannot be caused by the simple superposition of monoelemental NPs (for a more detailed discussion see Fig. S2 in the Supporting Information). Moreover, a peak is developed around 410 nm associated to the SPR of silver. As expected, the intensity of this peak increases with the silver content due to a major extinction cross section associated to silver. This could be originated by the growth of the silver shell over the Au NPs but may be also associated to the formation of Ag NPs. TEM images (Fig. 2b–d) reveal that the silver deposit is not homogeneously distributed neither along a single NP surface nor between particles.

Also, Ag NPs presence is observed for the higher AgNO_3 concentrations (0.03 mM and 0.04 mM, c and d images respectively). As described in the experimental section, Ag NPs nucleation does not occur in the baths for at least a couple of hours despite the presence of the precursor (AgNO_3) and the reducing agent (H_2Q). This is due to the acidic nature of the solution where nucleation by H_2Q is kinetically inhibited [33]. This analysis leads to a question: why Ag NPs are formed after the seeding? A possible answer can be proposed by considering the presence of chloride anions coming from the gold precursor employed (HAuCl_4) that remain in the solution of the gold seeds. The chloride ion concentration in the baths after seeding is 0.08 mM; this is enough to trigger AgCl precipitation for

AgNO_3 concentration values higher than 0.002 mM. So it is reasonable to think that AgCl precipitation occurs simultaneously with the reduction reaction driving to Ag NPs formation by heterogeneous nucleation over the AgCl nuclei.

The blue shift in the SPR associated with gold indicates the formation of the silver shell on the Au NPs [14–16], however, it does not provide any direct information about the size and shape of such shell. In addition, by analyzing spectroscopic results only, it is not possible to clearly distinguish how Ag NPs and Ag shells do contribute to the extinction peak around 410 nm. Furthermore, TEM analysis allows to obtain direct evidence of the silver shell and the Ag NPs formation, although getting quantitative information is harder due to the variety of nano-objects in the samples (Ag NPs and Au@Ag NPs with different size, shape and composition). In such heterogeneous system, the poor sampling conditions in TEM (NPs analyzed less than $1 \times 10^{-5}\%$) make a statistical analysis unreliable; therefore, a more detailed TEM characterization would not contribute significantly to the analysis. In what it seems a dead end with conventional techniques, MEIS represents an attractive alternative to the classical morphological analysis, as it will be shown below.

Fig. 3a shows the MEIS scattered intensity of the mentioned four samples, normalized by the intensities of the Au peaks at the scattered angle of 131° . The intensities from the backscattering at Au and Ag atoms are indicated in the figure as well as the energy position corresponding to Au and Ag atoms at the surface. If compared with the signal of the Au NPs seeds (red line) it can be noticed that, the presence of Ag (i) affects the shape of the Au peak and, also, it (ii) causes an average energy shift of about 1.5 keV for the Au signal, which was taken comparing the highest energy value at the half maximum intensity. These observations constitute a clear evidence of the Ag deposition on the Au NPs surface. In addition, (iii) the signal corresponding to Ag atoms starts from an energy of about 134.3 keV, the backscattering energy for Ag atoms located at the surface. Since those three features are well known as been typical for core@shell NPs [26,28], it indicates the formation of a compound NP with a Ag shell and a Au core.

From the areas of the Ag and Au MEIS signals in Fig. 3a, the total amount of Ag relative to the total amount of Au atoms was determined. This ratio is presented in Fig. 3b as a function of AgNO_3 bath concentration. As expected from the experimental conditions and the spectroscopic results, the Ag atoms proportion increases with the AgNO_3 concentration. It is important to point out that the ratios determined by MEIS are related to the macroscopic stoichiometry of the whole sample and not necessarily to the individual composition of the NPs. So, similar with the spectroscopic analysis, it is not possible to determine from the elemental composition if the silver is forming shells or Ag NPs. In Fig. 3b are also represented the Ag/Au ratio calculated directly from the concentrations used in the experiments. It is clear that the experiment and MEIS ratios diverge for increasing AgNO_3 concentration. This may be related to the sample preparation; it is possible that Ag NPs formed at high AgNO_3 concentrations (Fig. 2c and d) adsorb on the substrate in a higher proportion than Au@Ag NPs in respect to that of the solution and, as a consequence, silver composition is higher on the wafers. This is also consistent with the increasing discrepancy in the elemental composition with AgNO_3 concentration between MEIS and the experiment since at higher AgNO_3 concentration more AgCl precipitation is expected and thus, more Ag NPs are supposed to be formed.

Up to this point, MEIS analysis allows to have complementary evidence to the main observations drawn from the conventional techniques. Nevertheless, as will be shown below, a quantitative analysis of these polydisperse samples can be made through the modeling of MEIS signals. This allows to go deeper into the analysis of the NPs obtained and, consequently, gain in understanding

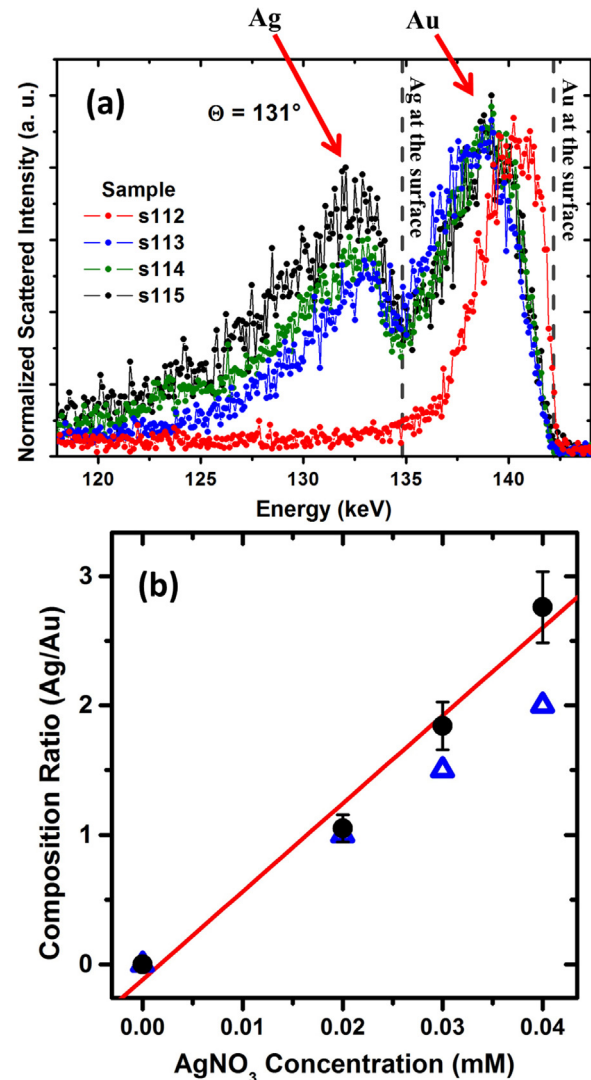


Fig. 3. (a) MEIS scattered intensity for samples s112–s115, normalized by the intensities of the Au peaks at the scattered angle of 131° . The vertical dashed lines correspond to the energies where Au and Ag are at the surface. (b) Total amount of Ag relative to Au atoms measured by MEIS (black dots) and calculated directly from the used concentrations in the synthesis (blue triangles) for each sample studied here and the MEIS linear fitting (red line). (For interpretation of the references to colour in this figure legend, the reader is referred to the web version of the article.)

about the process involved in their synthesis. Here we have used the sample s112, without Ag, as a reference to characterize later the core–shell structure of the other samples. The size of the NPs on sample s112 was also determined by MEIS analysis. Simulations of the MEIS spectra at different scattering angles were performed by using the PowerMEIS code [29]. In order to assess the influence of qualitative features of the sample on the MEIS simulations, all Au NPs were considered as spheres in consistency with the TEM analysis. The sphere radius was assumed as an adjustable parameter in a range of values that includes the average radius estimated from TEM.

The simulated spectra were compared with the measured ones at three different scattered angles: 109° , 120° and 131° (shown in Fig. 4a–c), assuming as figure of merit for the fitting quality, the reliability criteria R^2 [20] that reads

$$R^2 = \frac{1}{N} \sum_{i=1}^N [I(r)_{\text{Sim},i} - I_{\text{Exp},i}]^2, \quad (1)$$

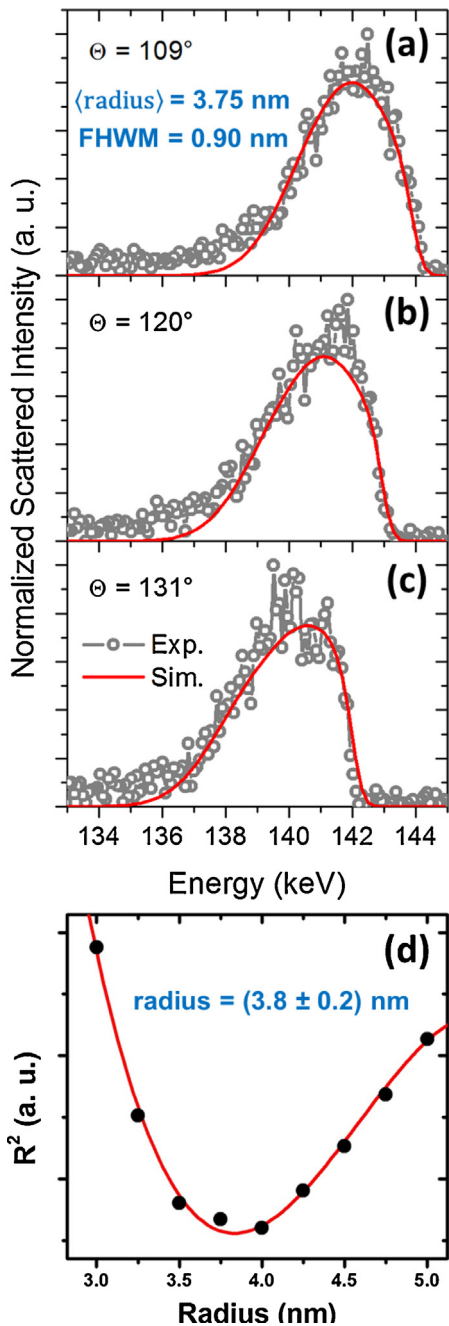


Fig. 4. (a–c) Simulated MEIS spectra (red lines) compared to the measured ones (grey line-open circles) at three different scattered angles for the sample s112. (d) R^2 values (full black circles) as a function of the Au NPs radius and the cubic polynomial regression fit (red line). The mean radius and its statistical error of 3.8 and 0.2 nm, respectively, were obtained from this polynomial fitting. (For interpretation of the references to colour in this figure legend, the reader is referred to the web version of the article.)

where $I(r)_{\text{Sim},i}$ and $I_{\text{Exp},i}$ correspond to the simulated, for a radius r , and experimental ion scattering intensities respectively, and N to the number of angles. For each scattering angle, the energy window was selected to correspond with the Au signal only. Fig. 4d shows the reliability values as a function of the radius of the Au NP, where the full circles correspond to simulations and the line is a cubic polynomial fitting. Hence, the best fitting is given by the minimum of the reliability function, corresponding to a radius of 3.8 nm.

The size distribution of the NPs was estimated also from the R^2 criteria. In this case, the fitting of the experimental data was made

by considering a linear combination of the simulated MEIS spectra for different radii of NPs. A finite set of simulated NPs spectra was considered varying the radii of NPs in the range of 3.0–5.0 nm with a 0.5 nm interval. The TEM size distribution was used to set the initial values of the coefficients of the linear combination. A minimization of R^2 was made by varying the weights of each simulated spectra, where the linear coefficients were optimized with the only restraint that they should remain positive. The minimum R^2 value was obtained for a radius of (3.8 ± 0.4) nm.

Since the Au NPs sample is nearly-monodisperse, the statistical analysis based on TEM images is reliable and a direct comparison with MEIS results is possible. The estimation of the mean radius $\langle r \rangle$ from the analysis of MEIS data falls into the interval $\langle r \rangle \pm \sigma$ obtained from TEM images statistical analysis (2.9–4.1 nm), within a difference between both values of $\langle r \rangle$ as high as the 9%. This similarity between the $\langle r \rangle$ values reveals the consistency of both analyses, making them reliable. It also indicates that the starting assumption made on by considering Au NPs to be spheres in order to analyse MEIS data is quite reasonable. The importance of such a result is stressed when particular aspects of TEM and MEIS are regarded. These techniques operates under sampling conditions which are quite different, given that the typical TEM sample area can be 10^8 times smaller than the MEIS one. In particular, MEIS signal is more sensitive to the bigger NPs, since they contain many more atoms. The proximity between neighboring or near-overlapping NPs is also a feature to consider, since this may cause an increasing of the energy loss straggling, which is more often associated with larger NPs. For this reason, the presence of NPs aggregates should be avoided in MEIS samples since that may be a source of artifacts in the characterization. Unlike in TEM, where sample preparation frequently consists in drying a drop of a colloidal solution, sample preparation in MEIS often requires a more elaborate methodology. In our particular case, NPs aggregation in MEIS samples is avoided since no drying is needed. The NPs are electrostatically bound to APTES amino terminal groups and, as is shown in Fig. S1, the NPs are homogenously distributed among the surface and no aggregates are observed.

MEIS results corresponding to Au@Ag NPs samples were analyzed by assuming that the addition of AgNO₃ does not modify the existing Au NPs morphology, as expected considering the experimental conditions. Several MEIS simulations for Au@Ag NPs were performed by setting the core radius (Au NPs) in 3.75 nm for different thicknesses of the Ag shell (Fig. 5a). It must be pointed out that the silver shell thicknesses cannot be determined directly by analysing the silver MEIS signal since Ag atoms do not form a homogenous spherical shell, as the TEM images indicates (Fig. 2b). Added to this, the possibility of Ag NPs presence in the samples makes the modelling of silver MEIS signal very complex because of the many parameters that would have to be adjusted. On the other hand, Au signal is only affected by the amount Ag that is deposited over the surface of the Au NPs. This makes the study of the Au signal much more convenient since it enables to leave aside from the analysis the Ag NPs, in the case they are present, and account for the Au@Ag NPs only. To exemplify these points, in Fig. 5b are shown the simulated MEIS spectra of a sample containing only Au@Ag NPs (pink line) and a sample containing monometallic Ag NPs and Au NPs (black line). As can be seen, if the silver is not deposited over the Au NPs but, instead, is forming Ag NPs, then the Au signal is the same as for the pure Au NPs (red line). If silver is deposited over the Au NPs surface, then, the Au signal is shifted to lower energies as compared to the pure Au NPs signal. Hence, in a sample containing a mixture of Au@Ag NPs and Ag NPs, the Au signal is only sensitive to the Au@Ag NPs.

As is evidenced in Fig. 5a, Au signal cannot be well fitted by considering only one single value of shell thickness. This is not surprising since TEM images clearly show that Ag shell is

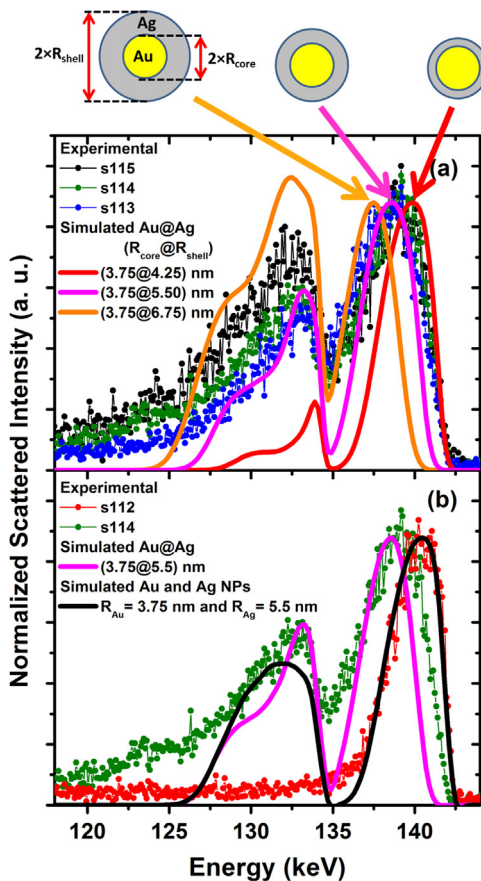


Fig. 5. MEIS spectra normalized by the intensities of the Au peaks at the scattered angle of 131° . (a) for the samples s113–s115 and simulated MEIS spectra for Au core radius of 3.75 nm and shell radius of 4.25, 5.5 and 6.75 nm, and (b) for the sample s114 and two simulated MEIS spectra: Au core radius of 3.75 nm and shell radius of 5.5 nm (in magenta) and a configuration of purely monometallic system of Au and Ag NPs with radius of 3.75 and 5.5 nm, respectively (in black), where the same overall stoichiometry was kept for those two configurations. (For interpretation of the references to colour in this figure legend, the reader is referred to the web version of the article.)

not homogeneously distributed as mentioned before. Hence, to properly fit the Au signals, a Ag thickness distribution has to be considered. Furthermore, the shape and position of the Au peak are nearly the same for the three samples with Ag (Fig. 6a), with energy differences as small as for an atomic Ag layer (0.2 keV or less). This necessarily implies that the Ag thickness distribution should be about the same for the three samples containing Au@Ag NPs (s113, s114 and s115). Therefore, a single fitting was performed over an average of the Au signals of the three samples. The R^2 function was minimized using a single linear combination of the simulated MEIS spectra with different shell width. The fitting procedure was very similar to that described for the Au NPs size distribution. To generate the set of simulated spectra, Au@Ag NPs were considered to be spherical, the Au core radius was set at 3.75 nm and the Ag shell thickness was vary between 0.0 nm (pure Au NPs only) and 5.0 nm with a 0.25 nm interval. It is important to notice that the non-homogeneous Ag shells are implicitly considered in the distribution since the spectrum for such a shell can be also represented by a linear combination of the spectra of spherical Ag shells. The best fitting to the Au signal of the experimental spectra is shown in Fig. 6a in a red solid line. The corresponding Ag shell thickness distribution for all samples is shown in Fig. 6b.

The similarities in the Ag shell distribution between the samples, as MEIS results show (Fig. 6a), indicate that the higher AgNO_3 concentration in samples s114 and s115 does not produce thicker

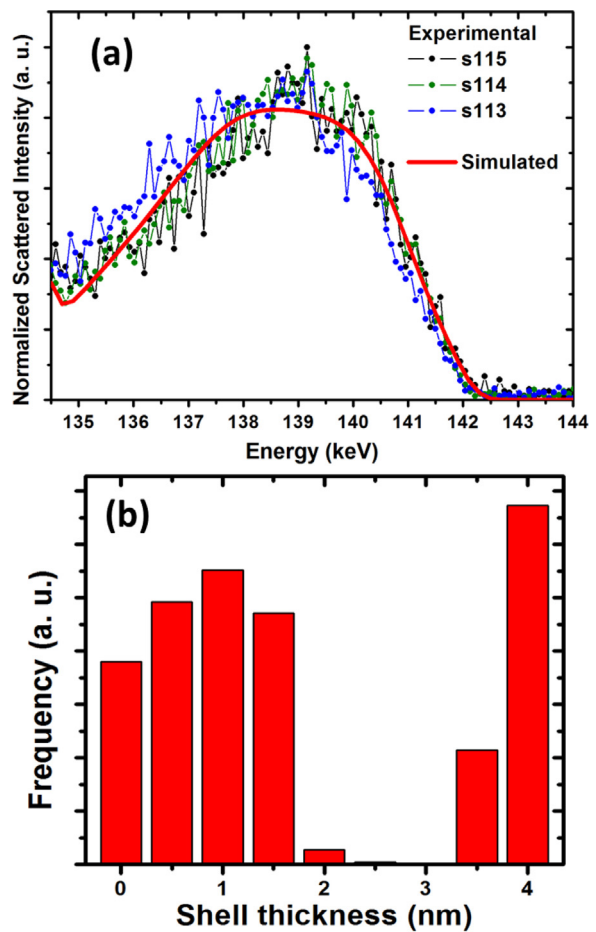
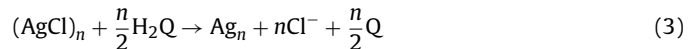


Fig. 6. (a) MEIS spectra in the Au peak energy range, normalized by the intensities of the Au peaks at the scattered angle of 131° for the samples s113–s115 (dots and lines) and simulated MEIS curve (red solid line) considering a Au core radius of 3.75 nm and the Ag shell thickness distribution shown in (b). (For interpretation of the references to colour in this figure legend, the reader is referred to the web version of the article.)

Ag shells than the one obtained in s113. Hence, the increase of the Ag SPR extinction in Fig. 2a so as the increase in the Ag proportion in MEIS (Fig. 3) is associated to a higher Ag NPs content and not to the presence of thicker Ag shells. The increase in the Ag NPs content with the rise in AgNO_3 concentration, instead of the Ag shell thickness growth, can be explained by considering two main reactions taking place at the same time:



where Reaction 2 corresponds to the growth of the silver shell and Reaction 3 is associated with the formation of Ag NPs from AgCl nuclei. As higher the initial AgNO_3 concentration is, Reaction 2 (shell thickness increase) goes faster as it is already known [34]. Nevertheless, Reaction 3 is more favored than Reaction 2 by the AgNO_3 concentration increase and, consequently, more AgNPs are formed instead of the silver shell growth.

In consistency with the heterogeneous shell distribution qualitatively observed by TEM, the Ag shell thickness distribution obtained from the Au MEIS signal fitting is bimodal (Fig. 6b). The histogram shows that there is a large portion of the Au NPs surface covered by a thin Ag layer of (1.0 ± 0.3) nm. The other contribution to the distribution corresponds to a proportion of Au NPs covered, or partially covered by approximately 4 nm of Ag. Although a

possible interpretation to the 3.5–4 nm contribution may be the attachment of small Ag NPs (radius ~2 nm) to the Au@Ag NPs surface, this can be neglected for two reasons: (i) TEM images show evidence of Ag shell thickness wider than 1 nm and (ii) MEIS samples are prepared by immersion and not by drying thus NPs aggregation should be minimum. The formation of such a heterogeneous Ag shell has its origin in differences in the Ag deposition kinetics. On one hand, silver deposition ratio may be dependent on the crystal faces exposed in the Au NPs seeds. Also, the size of the Au NP may play an important role since Ag UPD deposition has been reported to be favored on flatter Au surfaces [35–38]. Another issue to consider is that AgCl also deposit on the Au NPs and may affect the growth process. From the synthesis point of view, many factors that contribute to an uncontrolled shell growth may be easily minimized. For example, a possibility would be to decrease the Cl⁻/Ag⁺ ratio in order to prevent AgCl precipitation. Furthermore, as AgCl precipitation has a kinetic involve, it can be quenched by speeding up the reduction Reaction 2 raising H₂Q concentration. All these synthesis aspects have to be considered and are object of further investigations.

4. Conclusions

In this work, the Au@Ag NPs synthesized by a seed mediated procedure were systematically studied. The MEIS technique, recently developed to analyze NPs, has been successfully applied. Qualitative aspects such as Ag shell formation are unambiguously determined by this technique. Also quantitative information such as the Au NPs size and size dispersion ($r = (3.8 \pm 0.4)$ nm) were obtained in agreement with TEM determinations ($r = (3.5 \pm 0.6)$ nm). In addition, the sampling conditions ensure to have reliable information representative of the ensemble of NPs. This constitutes an advantage in relation to TEM, especially in samples which are morphologically and compositionally heterogeneous where TEM statistical analysis may become unreliable, which is the Au@Ag NPs current case. As MEIS analysis suggests, the Au@Ag NPs obtained have a non-homogeneous Ag layer with a bimodal thickness distribution. Also, no differences in the Ag thickness have been observed despite the increase in AgNO₃ concentration in the synthesis. Those two facts are associated to AgCl precipitation during Ag shell growth and their control is subject of further investigations.

Author contribution statement

RM, FPC and MAP worked on the sample synthesis. RM prepared all the samples for TEM and performed the TEM experiments as well. RM, PFPF and MAP worked on the discussions and analysis of TEM results. DFS, RM and MAP wrote the main manuscript text. RM prepared the first two figures; DFS prepare de others except the supplementary figure, which was prepared by RM and MAP. DFS planed and worked on the MEIS experiments, with the participation of PLG, PFPF and FPC. DFS worked on the MEIS analysis, with the participation of PLG and PFPF. All authors reviewed the manuscript.

Acknowledgments

The authors acknowledge the financial support by Brazilian agency CNPq, the PRONEX program, and the use of the infrastructure of the Ion Beam Implantation Laboratory at UFRGS. From the Argentinean side, the authors acknowledge the financial support of the Consejo Nacional de Investigaciones Científicas y Técnicas (CONICET) and the Secretaría de Ciencia y Tecnología (SECYT-UNC). The authors also thank the technical assistance from Claudia

Nome (IFFIVE) in TEM and from Daniel Brusa and Clemar Schürrer (CEMETRO-UTN) in AFM.

Appendix A. Supplementary data

Supplementary data associated with this article can be found, in the online version, at <http://dx.doi.org/10.1016/j.apsusc.2014.12.198>.

References

- [1] P. Sciau, Nanoparticles in ancient materials: the metallic lustre decorations of medieval ceramics, the delivery of nanoparticles, in: Abbass A. Hashim (Ed.), The Delivery of Nanoparticles, InTech, 2012, <http://dx.doi.org/10.5772/34080> (ISBN: 978-953-51-0615-9).
- [2] H.H. Park, K. Woo, J.-P. Ahn, Core–shell bimetallic nanoparticles robustly fixed on the outermost surface of magnetic silica microspheres, *Sci. Rep.* 3 (2013) 1497.
- [3] C.J. Serpell, J. Cookson, D. Ozkaya, P.D. Beer, Core@shell bimetallic nanoparticle synthesis via anion coordination, *Nat. Chem.* 3 (2011) 479–483.
- [4] S. Hwang, S.J. Yoo, J. Shin, Y.H. Cho, J.H. Jang, E. Cho, Y.E. Sung, S.W. Nam, T.H. Lim, S.C. Lee, S.K. Kim, Supported core@shell electrocatalysts for fuel cells: close encounter with reality, *Sci. Rep.* 3 (2013) 1309.
- [5] N.-H. Cho, T.-C. Cheong, J.H. Min, J.H. Wu, S.J. Lee, D. Kim, J.-S. Yang, S. Kim, K.K. Young, S.-Y. Seong, et al., A multifunctional core–shell nanoparticle for dendritic cell-based cancer immunotherapy, *Nat. Nanotechnol.* 6 (2011) 675–682.
- [6] S. Alayoglu, A.U. Nilekar, M. Mavrikakis, B. Eichhorn, Ru–Pt core–shell nanoparticles for preferential oxidation of carbon monoxide in hydrogen, *Nat. Mater.* 7 (2008) 333–338.
- [7] M. Tsuji, M. Nishio, P. Jiang, N. Miyamae, S. Lim, K. Matsumoto, D. Ueyama, X.-L. Tang, Role of chloride ions in the formation of Au@Ag core–shell nanocrystal structures by using a microwave–polyol method, *Colloids Surf. A: Physicochem. Eng. Aspects* 317 (2008) 247–255.
- [8] D.M. Mott, D.T.N. Anh, P. Singh, C. Shankar, S. Maenosono, Electronic transfer as a route to increase the chemical stability in gold and silver core–shell nanoparticles, *Adv. Colloid Interface Sci.* 185–186 (2012) 14–33.
- [9] S. Pyne, P. Sarkar, S. Basu, G.P. Sahoo, D.K. Bhui, H. Bar, A. Misra, Synthesis and photo physical properties of Au @ Ag (core @ shell) nanoparticles disperse in poly vinyl alcohol matrix, *J. Nanopart. Res.* 13 (2011) 1759–1767.
- [10] K. Tedsee, T. Li, S. Jones, C.W.A. Chan, K.M.K. Yu, P.A.J. Bagot, E.A. Marquis, G.D.W. Smith, S.C.E. Tsang, Hydrogen production from formic acid decomposition at room temperature using a Ag–Pd core–shell nanocatalyst, *Nat. Nanotechnol.* 6 (2011) 302.
- [11] M.B. Cortie, A.M. Mc Donagh, Synthesis and optical properties of hybrid and alloy plasmonic nanoparticles, *Chem. Rev.* 111 (2011) 3713.
- [12] K.J. Mayor, C. De, S.O. Obare, Recent advances in the synthesis of plasmonic bimetallic nanoparticles, *Plasmonics* 4 (2009) 61.
- [13] C.J. De Santis, R.G. Weiner, A. Radmilovic, M.M. Bower, S.E. Skrabalak, Seeding bimetallic nanostructures as a new class of plasmonic colloids, *J. Phys. Chem. Lett.* 4 (2013) 3072.
- [14] R.H. Morris, L.F. Collins, Optical properties of multilayer colloids, *J. Chem. Phys.* 41 (1964) 3357.
- [15] L.M. Liz-Marzán, A.P. Philipse, Stable hydrosols of metallic and bimetallic nanoparticles immobilized on imogolite fibers, *J. Phys. Chem.* 99 (1995) 15120.
- [16] Y. Kim, R.C. Johnson, J. Li, J.T. Hupp, G.C. Schatz, Synthesis, linear extinction, and preliminary resonant hyper-Rayleigh scattering studies of gold-core/silver-shell nanoparticles: comparisons of theory and experiment, *Chem. Phys. Lett.* 352 (2002) 421.
- [17] G. Park, D. Seo, J. Jung, S. Ryu, H. Song, Shape evolution and gram-scale synthesis of gold@silver core–shell nanopolyhedrons, *J. Phys. Chem. C* 115 (2011) 9417.
- [18] M. Tsuji, H. Adachi, S. Sugiyama, H. Matsumura, R. Murai, Y. Takahashi, S. Murakami, T. Inoue, Y. Mori, K. Takano, A manipulating tool for protein microcrystals in solution using adhesive materials, *Cryst. Growth Des.* 6 (2006) 11801.
- [19] Z.Y. Li, J.P. Wilcoxon, F. Yin, Y. Chen, R.E. Palmer, R.L. Johnston, Structures and optical properties of 4–5 nm bimetallic AgAu nanoparticles, *Faraday Discuss.* 138 (2007) 363.
- [20] D.F. Sanchez, G. Marmitt, C. Marin, D.L. Baptista, G. Azevedo, M. de, P.L. Grande, P.F.P. Fichtner, New approach for structural characterization of planar sets of nanoparticles embedded into a solid matrix, *Sci. Rep.* 3 (2013) 3414.
- [21] D.F. Sanchez, F.P. Luce, Z.E. Fabrim, M.A. Sortica, P.F.P. Fichtner, P.L. Grande, Structural characterization of Pb nanoislands in SiO₂/Si interface synthesized by ion implantation through MEIS analysis, *Surf. Sci.* 605 (2011) 654–658.
- [22] J. Leveneur, D.F. Sanchez, J. Kennedy, P.L. Grande, G.V.M. Williams, J.B. Metson, B.C.C. Cowie, Iron-based bimagnetic core/shell nanostructures in SiO₂: a TEM, MEIS, and energy-resolved XPS analysis, *J. Nanopart. Res.* 14 (2012) 1149.
- [23] I. Konomi, S. Hyodo, T. Motohiro, Simulation of MEIS spectra for quantitative understanding of average size, composition, and size distribution of Pt–Rh alloy nanoparticles, *J. Catal.* 192 (2000) 11.
- [24] T. Okazawa, M. Kohyama, Y. Kido, Electronic properties of Au nanoparticles supported on stoichiometric and reduced TiO₂(110) substrates, *Surf. Sci.* 600 (2006) 4430.

- [25] P.D. Quinn, N.R. Wilson, S.A. Hatfield, C.F. McConville, G.R. Bell, T.C.Q. Noakes, P. Bailey, S.H. Al-Harthi, F.S. Gard, Composition profiles of InAs–GaAs quantum dots determined by medium-energy ion scattering, *Appl. Phys. Lett.* 87 (2005) 153110.
- [26] H. Matsumoto, K. Mitsuhashi, A. Visikovsky, T. Akita, N. Toshima, Y. Kido, Au(core)/Pd(shell) structures analyzed by high-resolution medium energy ion scattering, *Nucl. Instrum. Methods Phys. Res. Sect. B* 268 (2010) 2281.
- [27] J. Gustafson, A.R. Haire, C.J. Baddeley, Depth-profiling the composition of bimetallic nanoparticles using medium energy ion scattering, *Surf. Sci.* 605 (2011) 220–224.
- [28] M.A. Sortica, P.L. Grande, C. Radtke, L.G. Almeida, R. Debastiani, J.F. Dias, A. Hentz, Structural characterization of CdSe/ZnS quantum dots using medium energy ion scattering, *Appl. Phys. Lett.* 101 (2) (2012) 023110.
- [29] M.A. Sortica, P.L. Grande, G. Machado, L. Miotti, Characterization of nanoparticles through medium-energy ion scattering, *J. Appl. Phys.* 106 (2009) 114320.
- [30] D.F. Sanchez, F. Rodrigues, F.P. Luce, Z.E. Fabrim, G.de.M. Azevedo, G. Keller-mann, D.L. Baptista, P.L. Grande, P.F.P. Fichtner, MEIS, TEM and GISAXS investigation of buried Pb nanoislands in SiO₂/Si interface, *Appl. Surf. Sci.* 321 (2014) 80–85.
- [31] I. Horcas, R. Fernández, J.M. Gómez-Rodríguez, J. Colchero, J. Gómez-Herrero, A.M. Baro, WSXM: a software for scanning probe microscopy and a tool for nanotechnology, *Rev. Sci. Instrum.* 78 (2007) 013705.
- [32] C.F. Bohren, D.R. Huffman, *Absorption and Scattering of Light by Small Particles*, Wiley Interscience, New York, 1983.
- [33] M.A. Pérez, R. Moiraghi, E.A. Coronado, V.A. Macagno, Hydroquinone synthesis of silver nanoparticles: a simple model reaction to understand the factors that determine their nucleation and growth, *Cryst. Growth Des.* 8 (2008) 1377.
- [34] T.H. James, The reduction of silver ions by hydroquinone, *J. Am. Chem. Soc.* 61 (1939) 648.
- [35] O.A. Oviedo, E.P.M. Leiva, M.M. Mariscal, Thermodynamic considerations and computer simulations on the formation of core-shell nanoparticles under electrochemical conditions, *Phys. Chem. Chem. Phys.* 10 (2008) 3561–3568.
- [36] O.A. Oviedo, M.M. Mariscal, E.P.M. Leiva, On the occurrence of stable and super-saturated metastable states in metallic core-shell nanoparticles, *Phys. Chem. Chem. Phys.* 12 (2010) 4580.
- [37] M.M. Mariscal, O.A. Oviedo, E.P.M. Leiva, On the selective decoration of facets in metallic nanoparticles, *J. Mater. Res.* 27 (2012) 1777.
- [38] O.A. Oviedo, L. Reinaudi, E.P.M. Leiva, The limits of under potential deposition in the nanoscale, *Electrochem. Commun.* 21 (2012) 14.